

5. Convective-Stratiform Separation

This section summarizes the work performed in this reporting period toward development of a real-time convective-stratiform separation algorithm in support of VPR correction (Seo et al. 2000).

5.1 Introduction

In Seo et al. (2000), a need has been identified for development of a real-time convective-stratiform separation algorithm so that VPR correction (Seo et al. 2000) may be performed at all times regardless of the type of the storm on hand. In this section, we summarize the first-year effort toward developing such an algorithm. The primary objective of this year's work was to identify the variables/attributes/indices/measures that possess significant skill in convective-stratiform separation. The secondary objective was to identify the candidate techniques that may be used to objectively quantify the probability of a particular azimuth-range (azran) bin belonging to the convective core.

Before proceeding further, it must be pointed out here that, even though we freely use the terms “convective” and “stratiform” throughout this section, we are not necessarily interested in convective-stratiform separation in the storm-dynamical sense (see, e.g., Houze 1993, p197). Rather, our interest is strictly reflectivity-morphological: separate all instantaneous and azran bin-specific VPRs in the rain area into “convective” and “stratiform” groups such that VPR correction yields the largest margin of improvement in estimation of surface rainfall. It must also be noted here that, in addition to supporting VPR correction, convective-stratiform separation may also be used in application of region-specific Z-R parameters. This microphysical aspect of convective-stratiform separation (see, e.g., Houze 1993, p1999), however, cannot be effectively dealt with without VPR correction, and hence is not considered in this work.

5.2 Literature Review

Steiner et al. (1995) offers probably the most extensive review of the radar data-based convective-stratiform separation techniques. It is worth repeating their key findings here because they serve as our starting point:

- identifying stratiform precipitation by bright band signatures is severely limited,
- observation of bright band may, however, be used as a check on stratiform precipitation not being misidentified as convective,
- time continuity techniques (based on echo-tracking) are laborious and computationally expensive,
- use of the horizontal structure of precipitation field is simpler and more practical, and
- criteria for identifying convective precipitation include intensity, peakedness, and surrounding area.

From the viewpoint of WSR-88D VPR correction, the biggest limitations of Steiner et al. (1995) are seen to be the following:

- separation is performed on Cartesian-gridded reflectivity data at 3-km altitude, and hence only out to ranges of about 140 km, and
- a more rigorous and objective set of criteria is probably needed to prevent intense bright band enhancement (easily exceeding 40 dBZ) from being misidentified as convective.

TRMM (the Tropical Rainfall Measuring Mission) PR (the Precipitation Radar) employs two different methods to classify rain type; the vertical profile method and the horizontal pattern method of Steiner et al. (1995). Below, we reproduce the summary of the vertical profile method (<http://trmm.gsfc.nasa.gov/2a23.html>):

- bright band is detected based on the second derivative of reflectivity with respect to range, and by imposing several conditions on the shape of the bright band profile and uniformity of the height of the bright band peak, etc.,
- the height of the bright band must lie within ± 1.5 km of the climatological freezing level,
- when bright band exists, rain is stratiform,
- when bright band is not detected and the maximum reflectivity exceeds the convective threshold, rain is convective, and
- the rest is classified as non-stratiform and non-convective.

From the viewpoint of WSR-88D VPR correction, use of the climatological freezing level is clearly inadequate. Also, because bright band can be reliably identified only when enhancement is intense, a large area of mild bright band enhancement may go largely undetected (and hence VPR-uncorrected).

It is somewhat puzzling to note that not much attention has been given in the literature to using standard spatial statistics (e.g., those used in the Radar Echo Classifier, Kessinger et al. 1998) in convective-stratiform separation. It may be that the computational burden has been a discouraging factor. As will be seen, such statistics are extensively explored in this work.

In light of the above observations, the approach taken in this work is the following:

- first identify convective cores and then perform checks on bright band-enhanced areas not being misidentified as convective cores,
- derive variables/attributes/indices/measures from the volume-scan reflectivity data in their original polar format at the $1^\circ \times 1$ km resolution and out to 230 km, and
- consider, at least initially, only those variables that may be objectively quantified in an azimuth bin-specific manner (so that the probability of a particular azimuth bin belonging to the convective core may be estimated with a reasonably simple technique: see below).

5.3 Identification of Skillful Variables

In identifying variables that may possess significant skill in convective-stratiform separation,

we assumed in this work that only the volume-scan reflectivity data are available. It is acknowledged that the height of the freezing level may also be available from sounding, surface observations and/or model output. As illustrated below, such an information may indeed be used to guide estimation of bright band height from the volume-scan reflectivity data. As also shown below, however, it is difficult to make an objective use of the resulting information in an azran bin-specific manner. For this reason, we did not explicitly require in this work that the freezing level be known from an external source.

The following variables (at each 1°x1 km azran bin and mapped onto the 230x360 base tilt) are considered in this work:

- maximum apparent radar rain rate in the vertical, denoted as r_x ,
- local mean of r_x , denoted as m_{r_x} ,
- local standard deviation of r_x , denoted as σ_{r_x} ,
- σ_{r_x}/m_{r_x} , denoted as cv_{r_x} ,
- local spatial correlation coefficient of r_x along the radial direction at the lag distance of 1 km, denoted as $\rho_{r_x}(1|ra)$,
- local spatial correlation coefficient of r_x along the azimuthal direction at the lag distance of 1 km, denoted as $\rho_{r_x}(1|az)$,
- weighted (according to the sample size) average of $\rho_{r_x}(1|az)$ and $\rho_{r_x}(1|ra)$,
- $\max\{\rho_{r_x}(1|az), \rho_{r_x}(1|ra)\}$,
- $\min\{\rho_{r_x}(1|az), \rho_{r_x}(1|ra)\}$,
- $\max\{\rho_{r_x}(1|az) - \rho_{r_x}(1|ra), 0\}$,
- height of the top of the apparent convective core, denoted as h_t ,
- m_{h_t} ,
- σ_{h_t} ,
- cv_{h_t} ,
- $\rho_{h_t}(1|ra)$,
- $\rho_{h_t}(1|az)$,
- weighted average of $\rho_{h_t}(1|az)$ and $\rho_{h_t}(1|ra)$,
- $\max\{\rho_{h_t}(1|az), \rho_{h_t}(1|ra)\}$,
- $\min\{\rho_{h_t}(1|az), \rho_{h_t}(1|ra)\}$,
- $\max\{\rho_{h_t}(1|az) - \rho_{h_t}(1|ra), 0\}$,
- height of the maximum reflectivity in the vertical, denoted h_x ,
- m_{h_x} ,
- σ_{h_x} ,
- cv_{h_x} ,
- weighted average of $\rho_{h_x}(1|az)$ and $\rho_{h_x}(1|ra)$,
- $\max\{\rho_{h_x}(1|az), \rho_{h_x}(1|ra)\}$,
- $\min\{\rho_{h_x}(1|az), \rho_{h_x}(1|ra)\}$,
- $\max\{\rho_{h_x}(1|az) - \rho_{h_x}(1|ra), 0\}$, and
- height of the bright band, and area of the bright band enhancement as estimated by a variant of Smith (1986) and Seo et al. (1997) (see below).

The motivation for the maximum apparent radar rain rate in the vertical, r_x , is to detect the presence of convective core (reflectivity > 40 dBZ, an adaptable parameter) regardless of the stage of development of the convection (see, e.g., Houze 1993, p198). Examination of many volume scans at KINX (Tulsa, OK) and KHGX (Houston, TX) indicates that identification of convective core based on the magnitude of r_x works well, as long as there is no bright band enhancement. The motivation for the spatial statistics of the maximum apparent radar rain rate in the vertical, r_x , the height of the top of the apparent convective core, h_x , and the height of the maximum reflectivity, h_x , is to detect the stratiform region and, in particular, the area of bright band enhancement. The spatial correlation coefficients are examined in two directions (i.e., azimuthal and radial) under the presumption that, e.g., r_x might be better correlated in the azimuthal direction than in the radial in the area of bright band enhancement.

The local statistics for the ij -th azimuthal bin are calculated over an area that is i azimuthal bins wide and j radial bins long. The initial sensitivity analysis indicates that a reasonable choice for i and j may be between 5 and 7 for both. Because we are using the same choice of i regardless of the slant range, the averaging area at a close range is necessarily much smaller than that at a far range. This dependence of statistics on the averaging area (i.e., on the slant range) will have to be examined further. Likewise, because the arc length of the azimuthal bin is range-dependent, sample spatial correlation coefficients along the azimuthal direction can only be calculated at different lag distances. To convert the sample spatial correlation coefficients at varying spatial lag distances to those at 1 km, it is assumed in this work that the correlation function is negative exponential (with no nugget effect). This assumption will also have to be investigated further.

To screen the variables listed above, we used the following two cases extensively; the squall line of May 8-9, 1995, at KINX, and the extreme rainfall event of Oct 17-18, 1994, at KHGX. The overriding motivation for the use of these cases was that they are rather difficult examples of the separation problem and that we know where the true areas of convective cores and stratiform region are: the squall line allows a clear-cut visual separation of convective and stratiform areas and, in the Houston case, we know from the radar-gage analysis (Seo et al. 1996) where bright band enhancement is present (though difficult to tell visually).

Based on various types of visual and statistical analyses using Splus (MathSoft 1998), we identified the following three as the most skillful; r_x , $\min\{r_x |_{az} |_{ra}\}$, and $\min\{r_x |_{az} |_{ra}\}$. For notational brevity, we denote $\min\{r_x |_{az} |_{ra}\}$ and $\min\{h_x |_{az} |_{ra}\}$ as r_x and h_x , respectively. The particular skill that each of these variables brings to convective-stratiform separation may be best illustrated through the following examples.

5.4 Example 1

This is an archetypical southern-plains squall line with clear-cut convective front and trailing stratiform region. Fig 1 shows the field of r_x . Note the concentric arcs in the stratiform region due to bright band enhancement. Figs 2 and 3 show the fields of $r_x > 15$ and < 15 (mm/hr), respectively. They represent the convective core (Fig 2) and the apparent non-convective core (Fig 3) regions after the initial separation using r_x . Note that this simple screening works well in

the convective core. It fails, however, in the stratiform region because of intense bright band enhancement.

Fig 4 shows the field of r_x . Note that the stratiform region is characterized by larger values of r_x , particularly at far ranges due in part to beam widening. Figs 5 and 6 show the fields of $r_x > 0.96$ and $r_x < 0.96$, respectively. They represent the stratiform (Fig 5) and the apparent non-stratiform (Fig 6) regions. It may appear that the stratiform region could have been better identified with a smaller threshold value of r_x . Further examination, however, suggests that the threshold has to be chosen rather conservatively because smaller threshold values of r_x tend to result in the identified stratiform region intruding on the (true) convective cores.

Comparison between Figs 2 and 5 indicates that the area of bright band enhancement in Fig 2 can be negated by the r_x screening only partially. To screen out the area of bright band enhancement at close ranges, we turn to h_x . Fig 7 shows the field of h_x . Note that the convective core is characterized by highly variable h_x whereas the stratiform/bright band-enhanced region is characterized by rather uniform h_x . Fig 8 shows the field of h_t . Figs 9 and 10 show the fields of $h_t > 0.99$ and $h_t < 0.99$, respectively. They represent the stratiform/bright band (Fig 9) and the apparent non-stratiform/non-bright band (Fig 10) regions.

Figs 11 through 14 illustrate how each of the three variables, r_x , r_x , and h_t , contributes to isolation of the convective core.

Fig 11 - the r_x threshold is applied: a large area of intense bright band enhancement is misidentified as convective

Fig 12 - the r_x threshold is additionally applied: bright band enhancement at mid - to far ranges is now correctly identified as stratiform, but that at close range is still misidentified as convective

Fig 13 - the h_t threshold is additionally applied: bright band enhancement at the close range is now correctly identified as stratiform, but the convective core at the farthest range at the top of the radar umbrella is now misidentified as stratiform

Fig 14 - convective-stratiform separation after applying all three thresholds

It may be argued that the r_x screening does not contribute much, and that screening based only on r_x and h_t may be just as effective. On the other hand, h_t is a measure that is significantly more range-dependent than r_x due to the sparsity of the sampling interval of the radar beams in the vertical, and hence is subject to large uncertainties. As such, exclusive reliance on h_t for identification of stratiform region/area of bright band enhancement should probably be avoided. To assess the range dependence of these measures and their skill, further investigation is needed.

We now turn our attention to the question of what may be gained in convective-stratiform separation if the height of the freezing level is available from an external source. Fig 15 shows the locations of the “couplets” corresponding to Fig 1. The couplet locations in the figure mark the azran bins in the volume-scan reflectivity data projected onto the base tilt for which, for each azimuthal angle, the peak reflectivity (a proxy for the bright band peak in the vertical) is observed at approximately the same height between any two adjacent tilts (for details see Smith

1986, Seo et al. 1997). In the figure, the concentric clusters are associated with the bright band peaks observed in the lowest (located at the farthest range) to the highest (located at the closest range) tilts. The elongated cluster in the southeastern sector is associated with the convective core (misidentified as bright band by the couplet analysis).

Fig 16 shows the distribution of the height of the couplets from all azimuthal angles. Visually, it is easy to tell that the tight horizontal cluster along the altitude of approximately 3.5 km is associated with the bright band, and that the loose clusters above and below the bright band height are associated with the convective front. The two solid horizontal lines in the figure are the break points produced from a cluster analysis, in which the data points in the figure are asked to be grouped into three clusters. Visually, it is easy to tell that it is the middle cluster which is associated with the bright band.

By simply calculating the mean and standard deviation of the data points in the middle cluster, one may obtain a very good estimate of the height of the bright band and a measure of uncertainty associated with it, as shown in Fig 17 by the solid and dashed lines, respectively. Following such an analysis, it is then possible to screen out the misidentified couplets (i.e., those that are associated with the convective front), and produce an estimate of the area of intense bright band enhancement (by what amounts to “connecting the dots” of surviving couplet points in Fig 15), as shown in Fig 18. Note that Fig 18 compares well visually with the area of intense bright band enhancement seen in Fig 1, suggesting that such a map may serve as an additional screening criterion in convective-stratiform separation.

Experience suggests, however, that in an automatic mode it is rather difficult to ascertain which cluster is associated with the bright band and which are not (note that the skill level for this discrimination has to be extremely high, probably close to perfection, for the technique to be operationally viable). The problem is much more difficult if the area of intense bright band enhancement is relatively small. It is in this area of pointing to the right cluster that the externally-provided freezing level can be useful.

5.5 Example 2

The second example comes from the extreme rainfall event at KHGX occurred in Oct 17-18, 1994 (NWS 1995). Fig 19 shows a field of r_x in the middle of the event. It is convective everywhere except at the farthest ranges in the northeastern sector, where based on the gage-radar analysis (Seo et al. 1996) we know that bright band enhancement is present. To assess robustness of the screening criteria, we used in this example exactly the same adaptable parameter and threshold values as those used in Example 1. Fig 20 shows the field of r_x corresponding to Fig 19. Note that the r_x values are larger in the area of bright band enhancement. Fig 21 shows the field of h_t . The spotty nature of the field is due in part to the relatively high (i.e., for this event) cutoff of 40 dBZ used to determine the convective core in calculation of r_x and h_t . Figs 22 through 25 are completely analogous to Figs 11 through 14, respectively. Considering that there was no case-specific tuning of any kind, the results are encouraging.

5.6 Objective Quantification of Prob[the bin convective]

In the two examples given above, we limited ourselves, for the sake of demonstration, to simply applying the thresholds to arrive at the final field of convective-stratiform separation. In practice, however, such a “binary decision-based” approach is not very desirable because a single set of thresholds cannot possibly work consistently and reliably for all sites, for all seasons, and regardless of the radar calibration accuracy. For this reason, for the separation algorithm to be operationally viable it is necessary that the likelihood of a particular azran bin belonging to the convective core be objectively quantified on a continuous scale (rather than binary-mapped). One such commonly used scale is the probability measure, which we will adopt here also.

The objective then is to estimate the conditional probability, Prob[the azran bin convective $\mathbf{r}_x = r_x, r_x = r_x, h_t = h_t$], where the bold signifies that it is a random variable. Though not explicitly denoted as such, the above probability will also have to be conditioned on the slant range so that range dependence of the skill in $r_x, r_x,$ and h_t may be accounted for (e.g., h_t at close and far ranges is much less informative than that at the mid range because of the cone of silence and the sparse sampling of the radar beams in the vertical, respectively). To estimate the conditional probability, we may consider a number of different techniques;

- neural network,
- fuzzy logic,
- optimal linear estimation (in particular, techniques based on indicator variable transformation),
- Bayesian estimation (probably following variable transformation into multivariate normal), and
- direct empirical estimation of the conditional probability.

If the number of attributes can be kept to as small as three (e.g., $r_x, r_x,$ and h_t), direct empirical estimation of the conditional probability may be the most desirable (completely data-driven, unbiasedness guaranteed). If the number of attributes is larger (say, several), optimal (linear or Bayesian) estimation may be preferred (they approximate multivariate statistics with a set of bivariate statistics). If the number of attributes is more than several, neural network or fuzzy logic may have to be used (explicit statistical modeling becomes very difficult).

The choice of the technique depends additionally on answers to the following questions: 1) are the model parameters to be updated on line? (algorithmically desirable but operationally impractical: see below), and 2) is unbiasedness in probability critical? If the answer to the first question is “yes,” neural network, fuzzy logic, and Bayesian estimation become more difficult to implement because they will require on-line training and/or parameter estimation. If the answer to the second question is “no,” neural network and fuzzy logic become more attractive because, to produce only “reasonable” results, rigorous training and parameter estimation/updates may not be needed.

In reality, the answer to the first question is probably “no” because, other than the human forecaster manually performing convective-stratiform separation on a volume-scan by volume-scan basis (clearly a very difficult task in the current operational environment), it will not be possible to generate the truth field *on line*. For this reason, it is particularly important that the technique of choice be parsimonious so that processing of long-term Level II data for parameter

estimation (requiring manual convective-stratiform separation) may be avoided. The answer to the second question is probably “yes” because biasedness in probability results, e.g., in VPR correction being applied mistakenly to convective cores even though the adjustment factors are derived from the stratiform profile (an error of very damaging consequence). In this respect, the last three candidates are more appealing because they are by design unbiased estimators (this unbiasedness, however, is guaranteed only if the second-order statistics required can be accurately estimated, which in reality may or may not be met depending in particular on the sample size).

Given the above observations and the fact that as simple a screening as applying three thresholds produces as encouraging a result as seen in Figs 11 through 14 and through 22 through 25, optimal linear estimation based on indicator (i.e., binary) variable transformation is seen to be an attractive compromise. In this approach, one may estimate the conditional probability, $\text{Prob}[\text{the bin convective } \mathbf{r}_x = r_x, r_x = r_x, h_t = h_t]$, via:

$$\begin{aligned} & \text{Prob}[\text{the bin convective } \mathbf{r}_x = r_x, r_x = r_x, h_t = h_t] \\ & E[I_{\text{conv}} I_{r_x = i_{r_x}} I_{r_x = i_{r_x}} I_{h_t = i_{h_t}}] \\ = & E[I_{\text{conv}}] + w_{r_x k} (i_{r_x} - E[I_{r_x k}]) + w_{r_x l} (i_{r_x} - E[I_{r_x l}]) + w_{h_t m} (i_{h_t} - E[I_{h_t m}]) \end{aligned}$$

where

$$i_{\text{conv}} = \begin{cases} 1 & \text{if the bin of interest is in the (true) convective core} \\ 0 & \text{otherwise} \end{cases}$$

$$i_{r_x k} = \begin{cases} 1 & \text{if } r_x \text{ at the bin of interest exceeds the } k\text{-th threshold} \\ 0 & \text{otherwise} \end{cases}$$

$$i_{r_x l} = \begin{cases} 1 & \text{if } r_x \text{ at the bin of interest exceeds the } l\text{-th threshold} \\ 0 & \text{otherwise} \end{cases}$$

$$i_{h_t m} = \begin{cases} 1 & \text{if } h_t \text{ at the bin of interest exceeds the } m\text{-th threshold} \\ 0 & \text{otherwise} \end{cases}$$

Note that, by definition, we have $E[I_{\text{conv}}] = \text{Prob}[\text{the bin convective}]$, $E[I_{r_x k}] = \text{Prob}[r_x > k\text{-th threshold}]$, $E[I_{r_x l}] = \text{Prob}[r_x > l\text{-th threshold}]$, and $E[I_{h_t m}] = \text{Prob}[h_t > m\text{-th threshold}]$. The weights, $w_{r_x k}$, $w_{r_x l}$, and $w_{h_t m}$, are given by:

$$\begin{pmatrix} w_{r_x k} \\ w_{r_x l} \\ w_{h_t m} \end{pmatrix} = \begin{pmatrix} \text{Cov}[I_{r_x}, I_{r_x}] & \text{Cov}[I_{r_x}, I_{r_x}] & \text{Cov}[I_{r_x}, I_{h_t}] \\ \text{Cov}[I_{r_x}, I_{r_x}] & \text{Cov}[I_{r_x}, I_{r_x}] & \text{Cov}[I_{r_x}, I_{h_t}] \\ \text{Cov}[I_{r_x}, I_{h_t}] & \text{Cov}[I_{r_x}, I_{h_t}] & \text{Cov}[I_{r_x}, I_{h_t}] \end{pmatrix}^{-1} \begin{pmatrix} \text{Cov}[I_{r_x}, I_{\text{conv}}] \\ \text{Cov}[I_{r_x}, I_{\text{conv}}] \\ \text{Cov}[I_{r_x}, I_{\text{conv}}] \end{pmatrix}$$

$$\begin{bmatrix} \text{Cov}[I_{ht}, I_{rx}] & \text{Cov}[I_{ht}, I_{rx}] & \text{Cov}[I_{ht}, I_{ht}] \\ \text{Cov}[I_{ht}, I_{rx}] & \text{Cov}[I_{ht}, I_{rx}] & \text{Cov}[I_{ht}, I_{ht}] \\ \text{Cov}[I_{ht}, I_{conv}] & \text{Cov}[I_{ht}, I_{conv}] & \text{Cov}[I_{ht}, I_{conv}] \end{bmatrix}$$

where, e.g., $\text{Cov}[I_{rxk}, I_{rxl}]$ is given, by definition, by $\text{Prob}[r_x > k\text{-th threshold}, r_x > l\text{-th threshold}] - \text{Prob}[r_x > k\text{-th threshold}]\text{Prob}[r_x > l\text{-th threshold}]$ (i.e., the centered bivariate probability).

The indicator approach is intuitive, and can accommodate both off-line parameter estimation and on-line parameter updating. A known drawback, however, is that the estimate becomes biased near the tail ends of the distribution if the variables involved are highly skewed (as r_x , r_x , and I_{ht} are). This, however, is probably not an issue in convective-stratiform separation because, for purposes of binary classification (i.e., either convective or stratiform), unbiasedness in probability is critical only near the median.

5.7 Conclusions and Recommendations

- Three variables have been identified as particularly skillful in convective-stratiform separation; the maximum apparent rain rate in the vertical, the local spatial correlation coefficient of the maximum apparent rain rate in the vertical, and the local spatial correlation coefficient of the height of the top of the apparent convective core.
- The initial results, obtained by simple application of the three thresholds, are very encouraging. It suggests that optimal linear estimation based on indicator variable transformation is well-suited for probabilistic quantification of convective-stratiform separation. It is proposed that such a procedure be prototyped and evaluated.
- The variables examined and identified as promising in this work need to be further tested against a wide spectrum of precipitation events. Also, the search for other potentially skillful variables needs to continue.
- Generation of validation data sets remains a critical outstanding issue. Manual mass-generation (eventually at the WFO's?) based on visual examination of volume-scan reflectivity data is not only labor-intensive but will also require a graphical user interface (GUI) tool (WATADS?). A user operations concept needs to be developed for VPR correction (including convective-stratiform separation) to address such issues.

References

- Houze, R. A., Jr., 1993: Cloud dynamics. Academic Press, Inc.
- Kessinger, C., S. Ellis, J. Van Andel, D. Ferraro, and R. J. Keeler, 1998: NEXRAD data quality optimization, FY98 Annual Report. NCAR, Boulder, CO.
- MathSoft, 1998: S-PLUS5. MathSoft, Inc., Seattle, WA.
- NWS, 1995: Natural Disaster Survey Report, Southeast Texas tropical mid-latitude rainfall and flood event, October 1994. DOC/NOAA/NWS Southern Region, Jan 1995.
- Seo, D.-J., R. Fulton, J. Breidenbach, M. Taylor, and D. Miller, 1996: Final Report, Interagency MOU among the NEXRAD Program, WSR-88D OSF, and NWS/OH/HRL. HRL/OH/NWS,

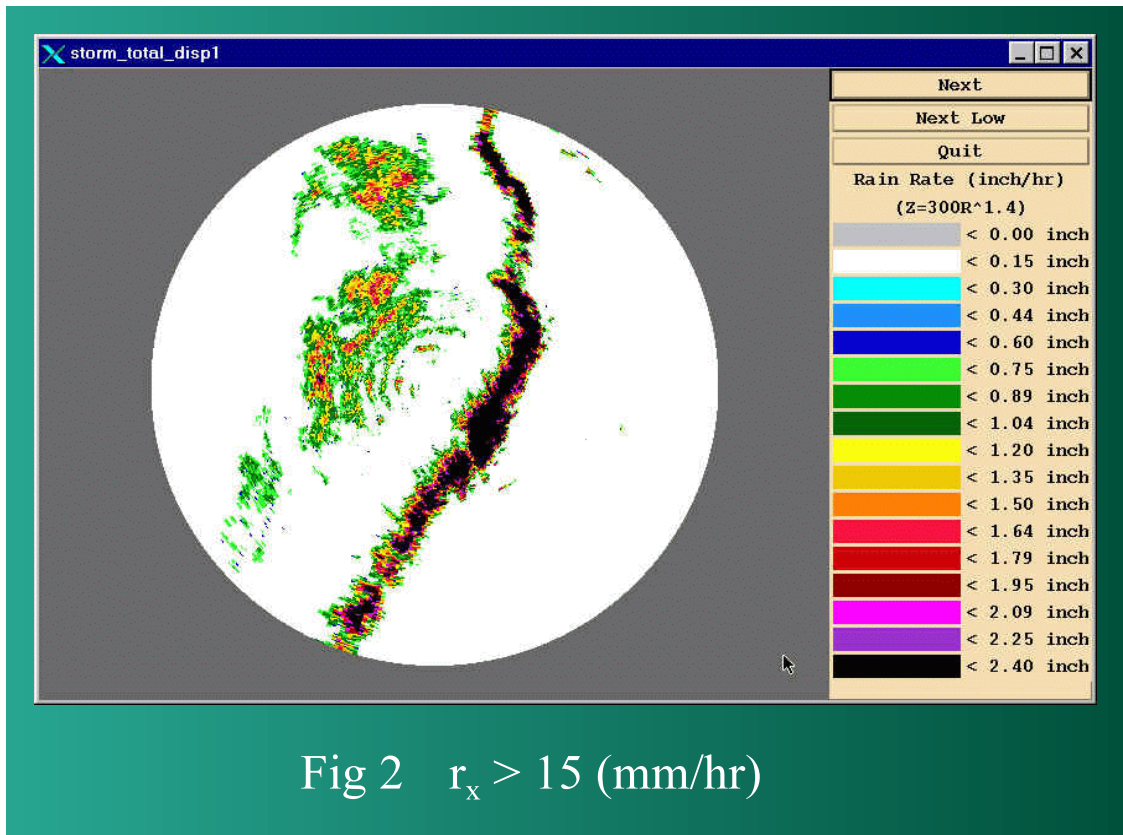
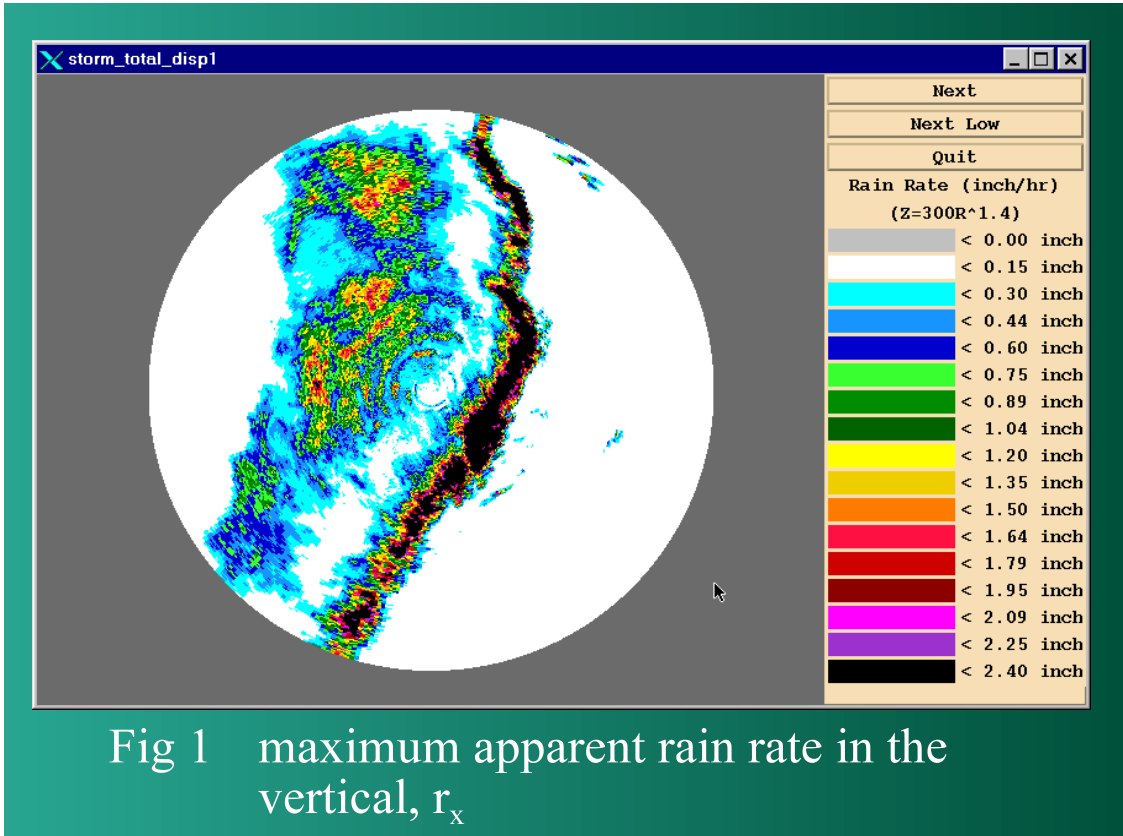
Silver Spring, MD.

Seo, D.-J., R. Fulton, J. Breidenbach, 1997: Final Report, Interagency MOU among the NEXRAD Program, WSR-88D OSF, and NWS/OH/HRL. HRL/OH/NWS, Silver Spring, MD.

Seo, D.-J., J. Breidenbach, R. Fulton, D. Miller, and T. O'Bannon, 2000: Real-time adjustment of range-dependent biases in WSR-88D rainfall estimates due to nonuniform vertical profile of reflectivity. *J Hydrometeorol*, 1(3), 222-240.

Smith, C. J., 1986: the reduction of errors caused by bright bands in quantitative rainfall measurements made using radar. *J. Atmos. Oceanic Technol.*, 3, 129-141.

Steiner, M. R., R. A. Houze Jr., and S. E. Yuter, 1995: Climatological characterization of three-dimensional storm structure from operational radar and rain gauge data. *J. Appl. Meteor.*, 34, 1978-2007.



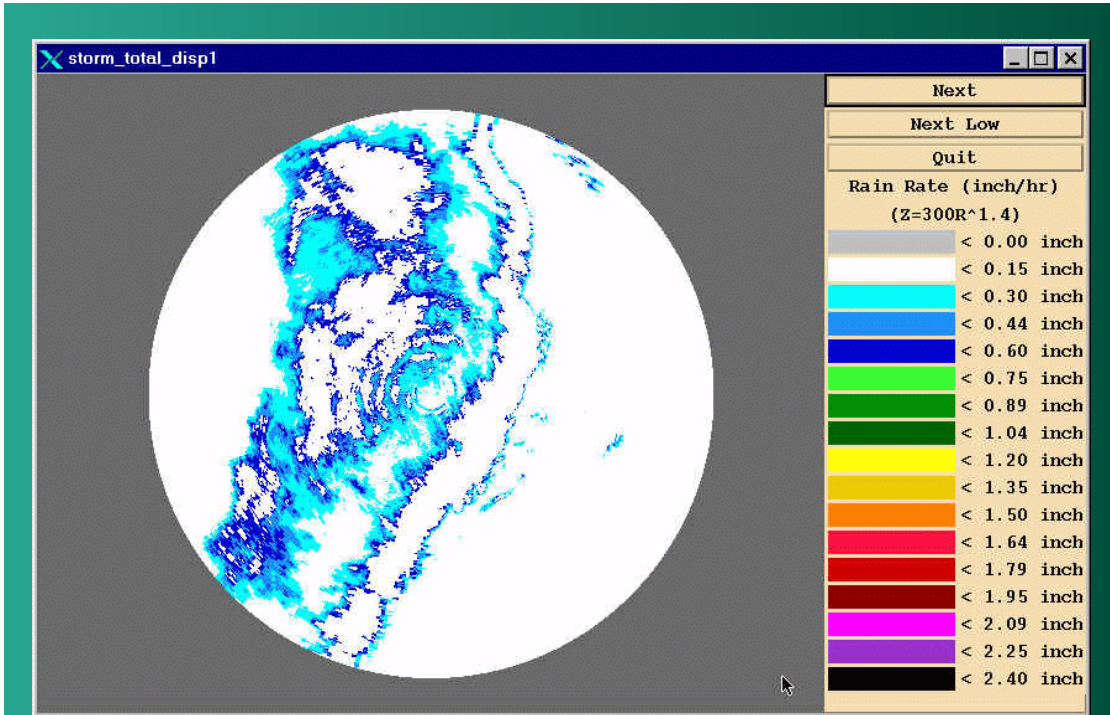


Fig 3 $r_x < 15$ (mm/hr)

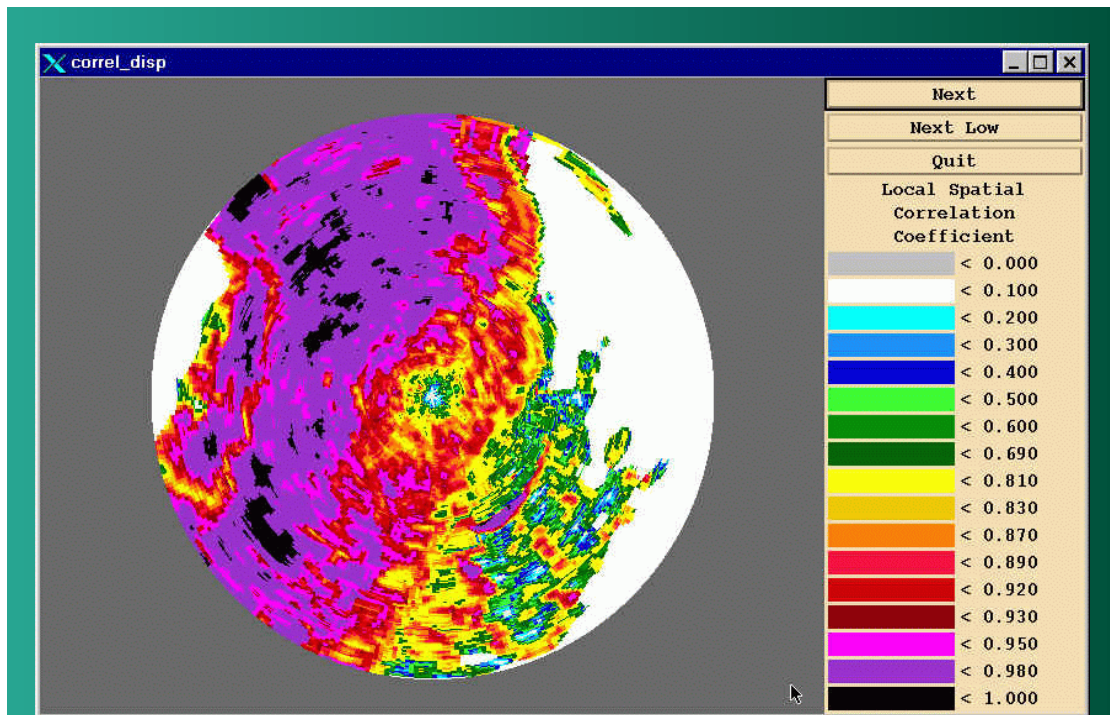
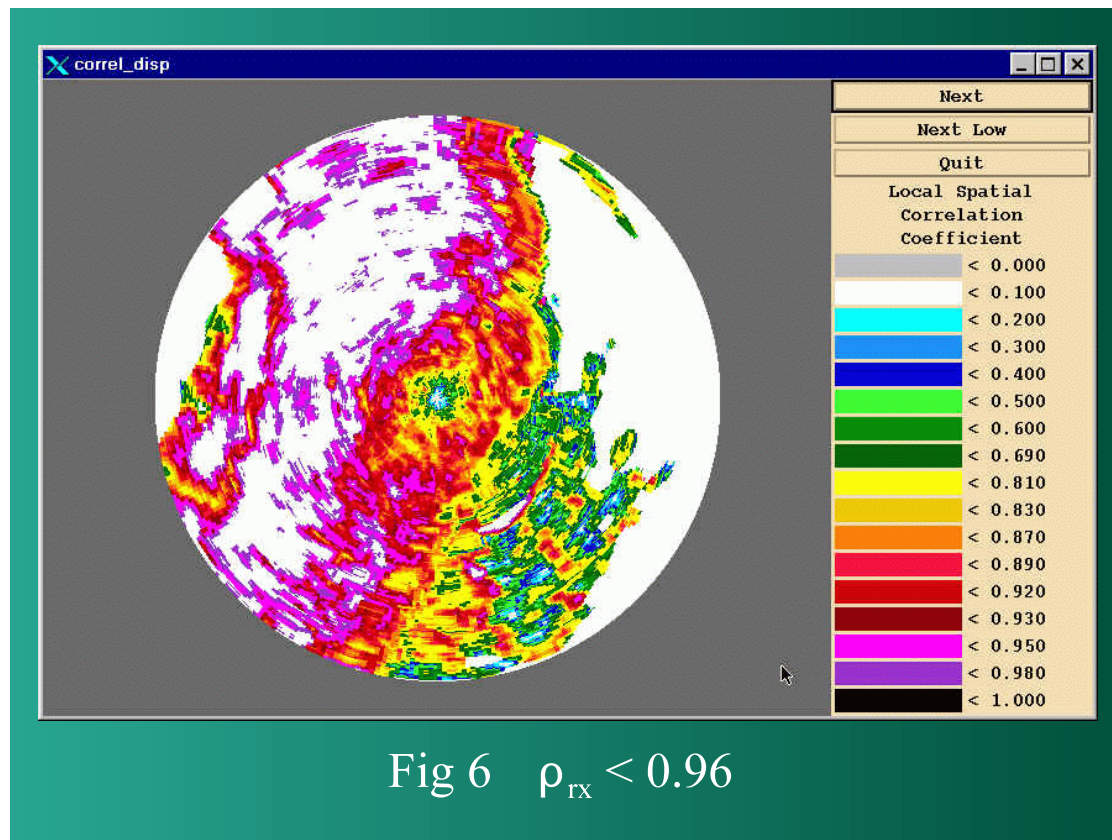
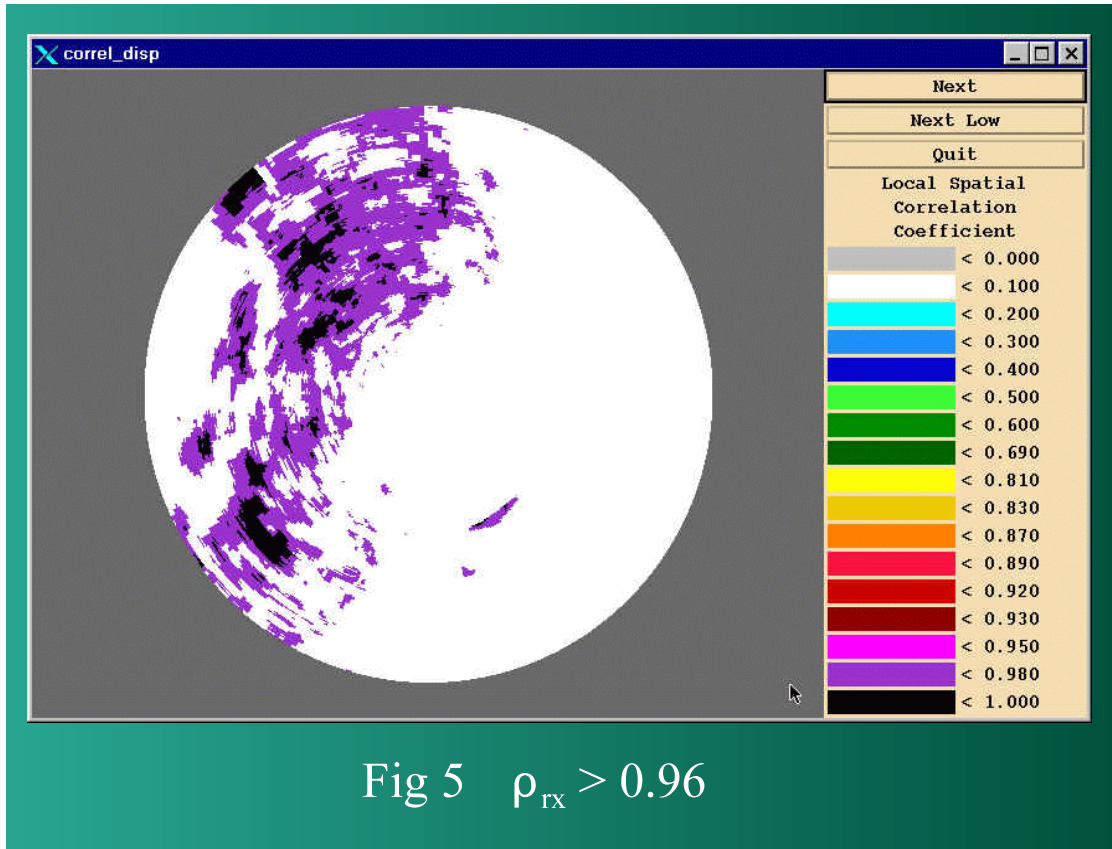
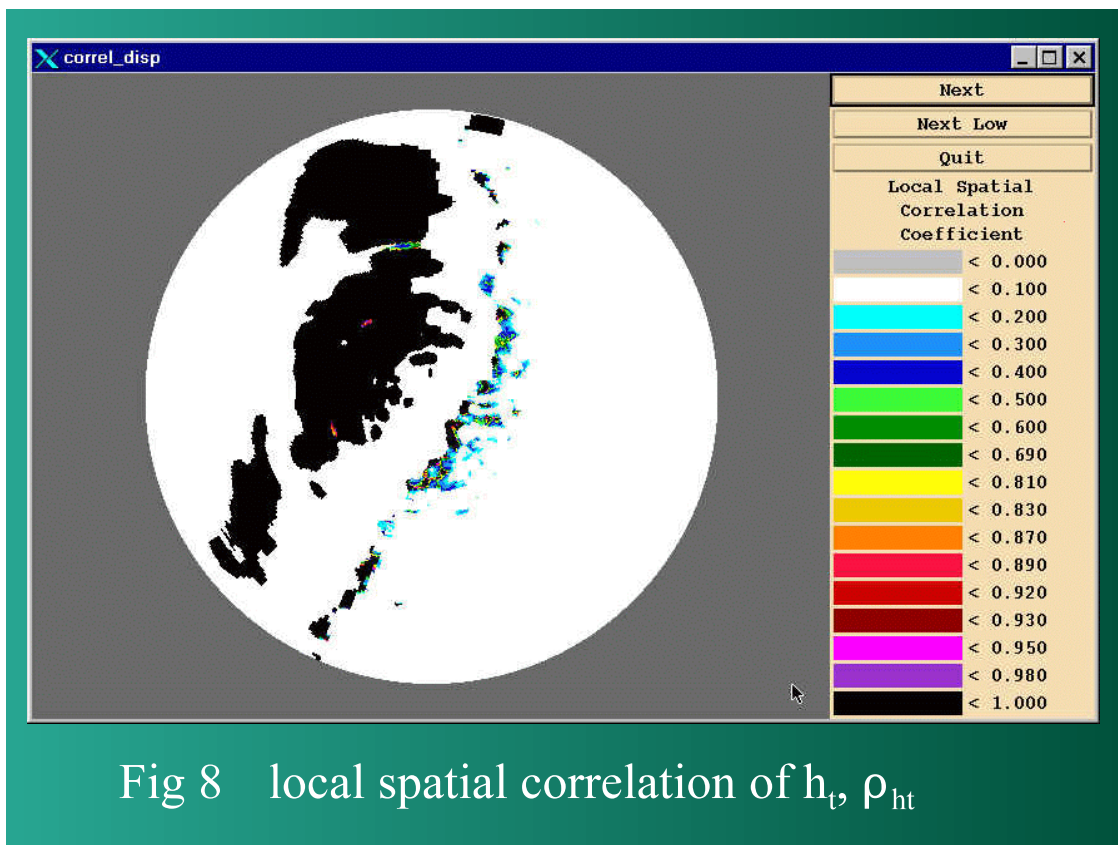
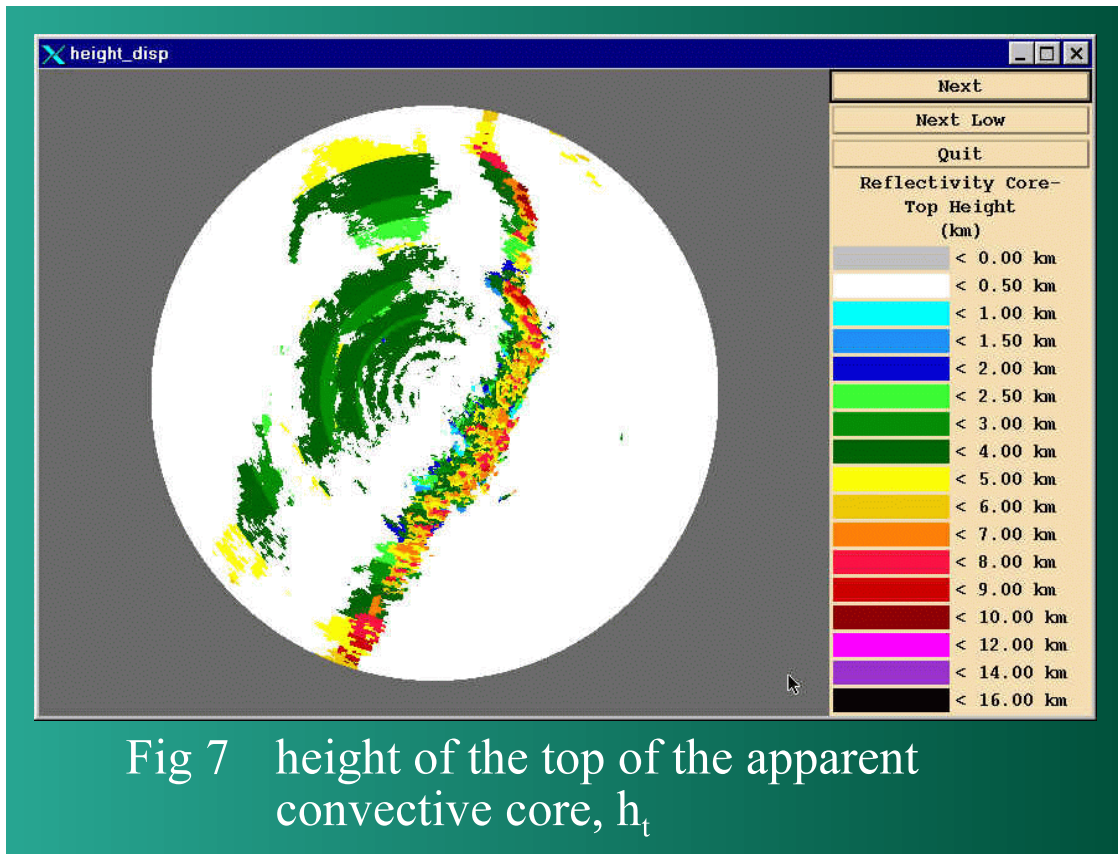


Fig 4 local spatial correlation of r_x, ρ_{rx}





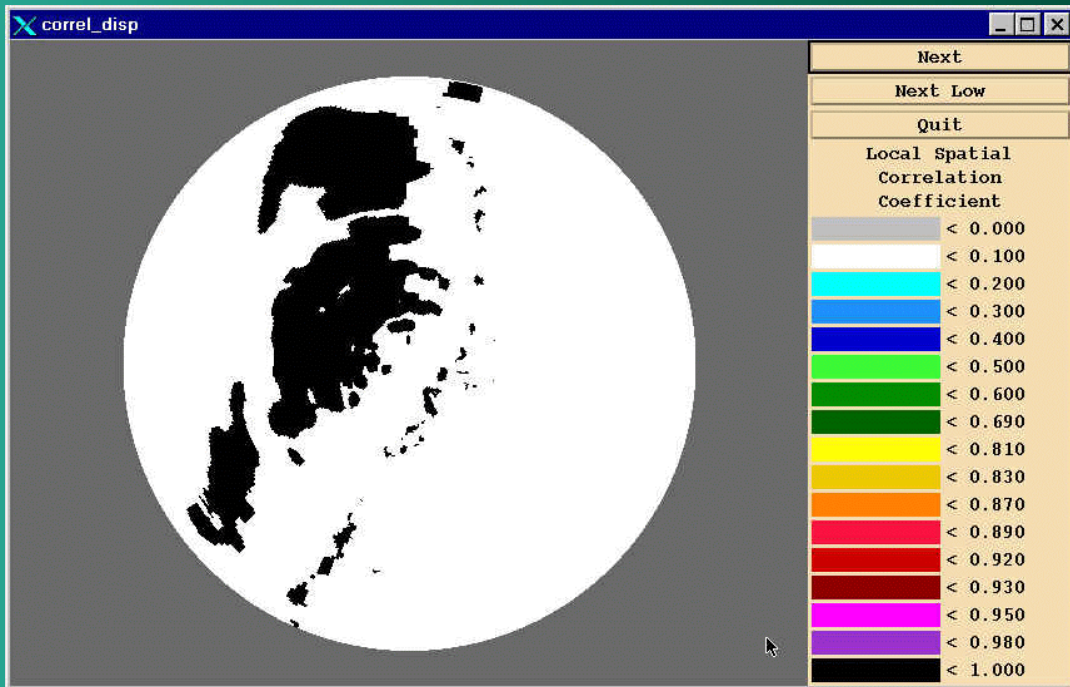


Fig 9 $\rho_{ht} > 0.99$

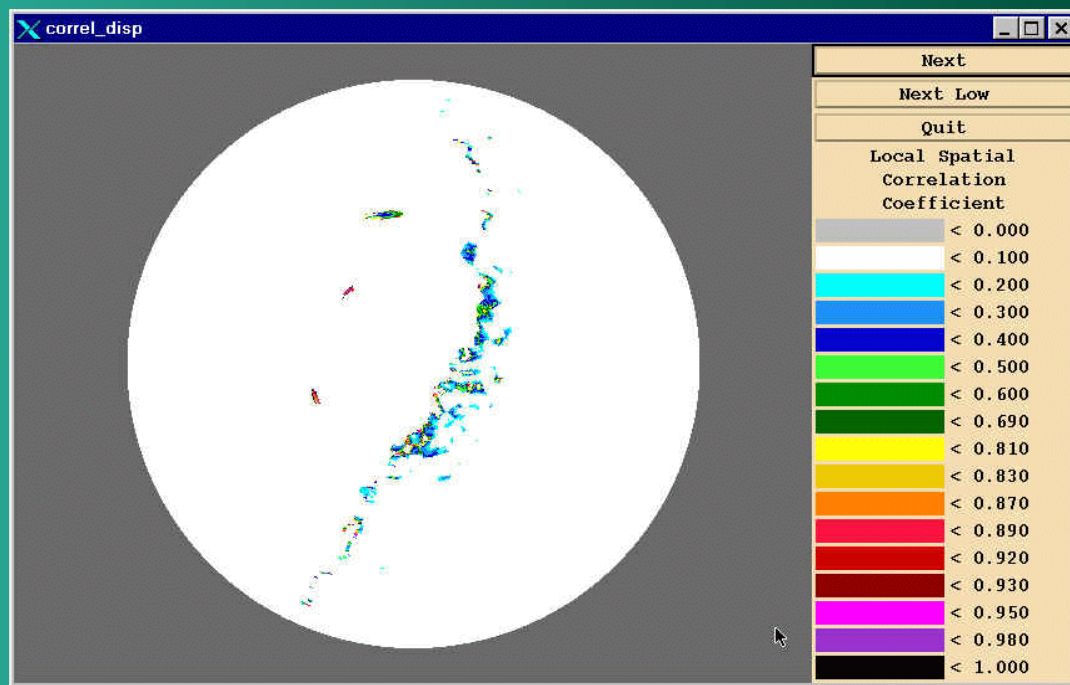
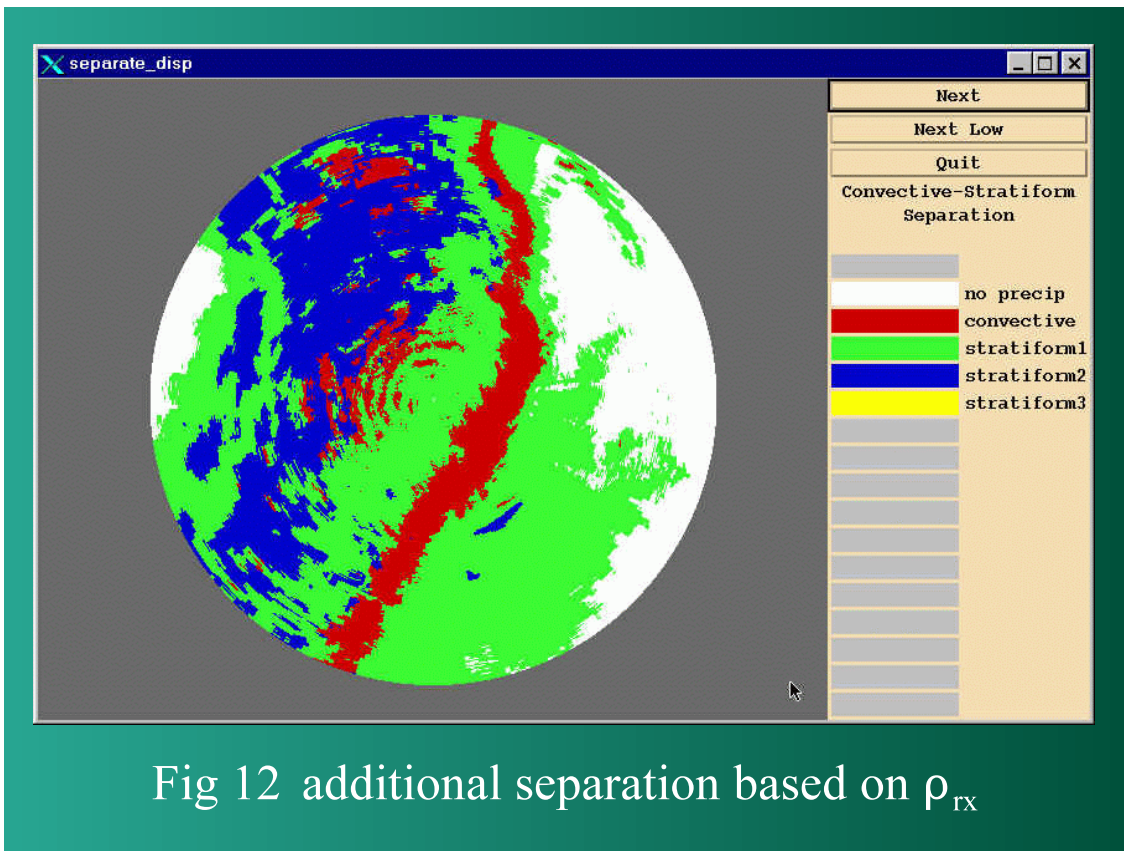
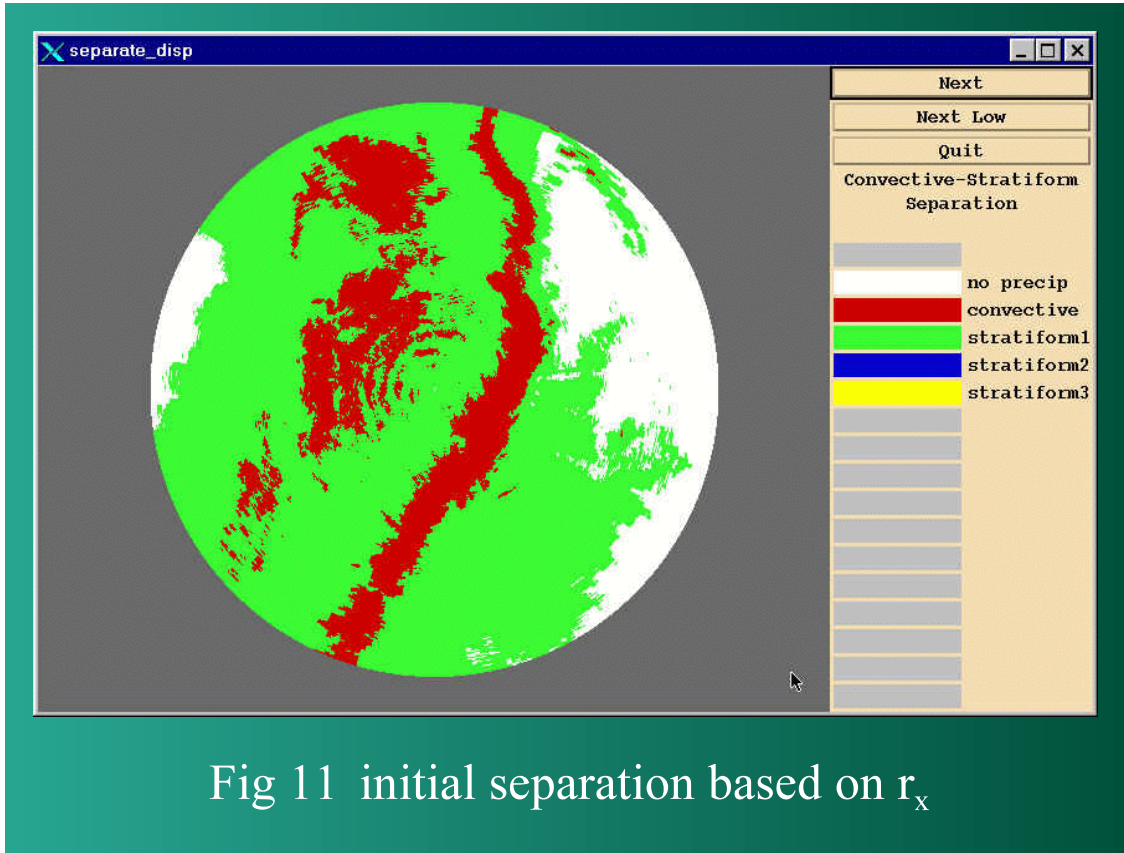


Fig 10 $\rho_{ht} < 0.99$



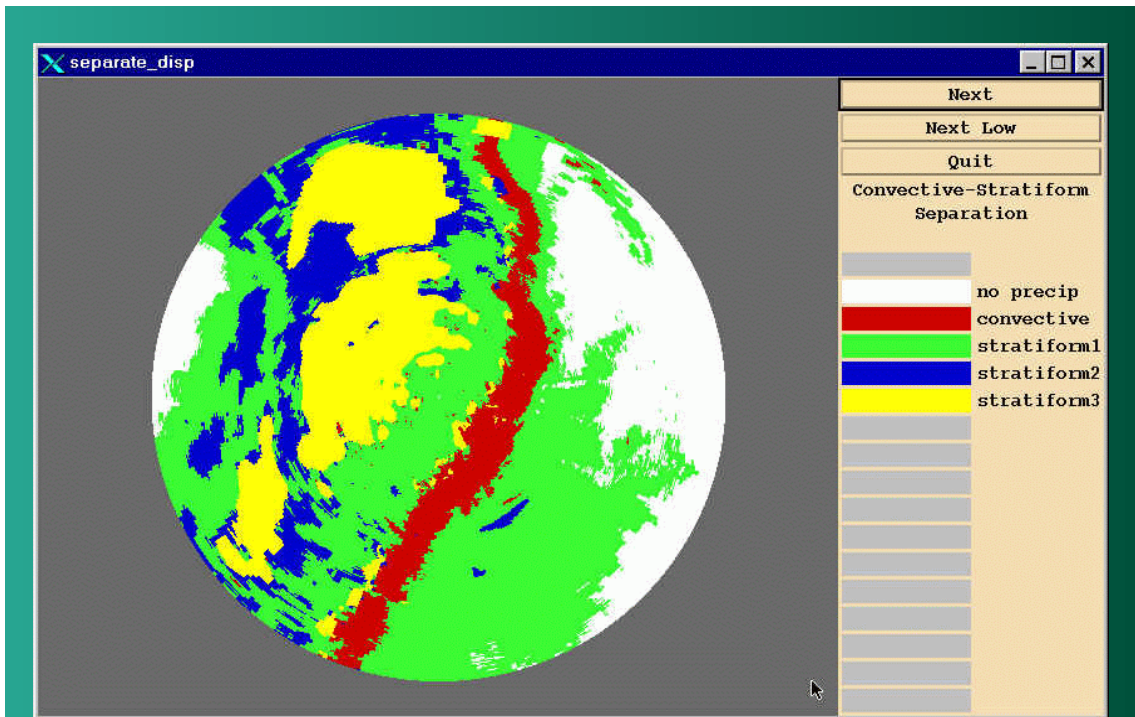


Fig 13 additional separation based on ρ_{ht}

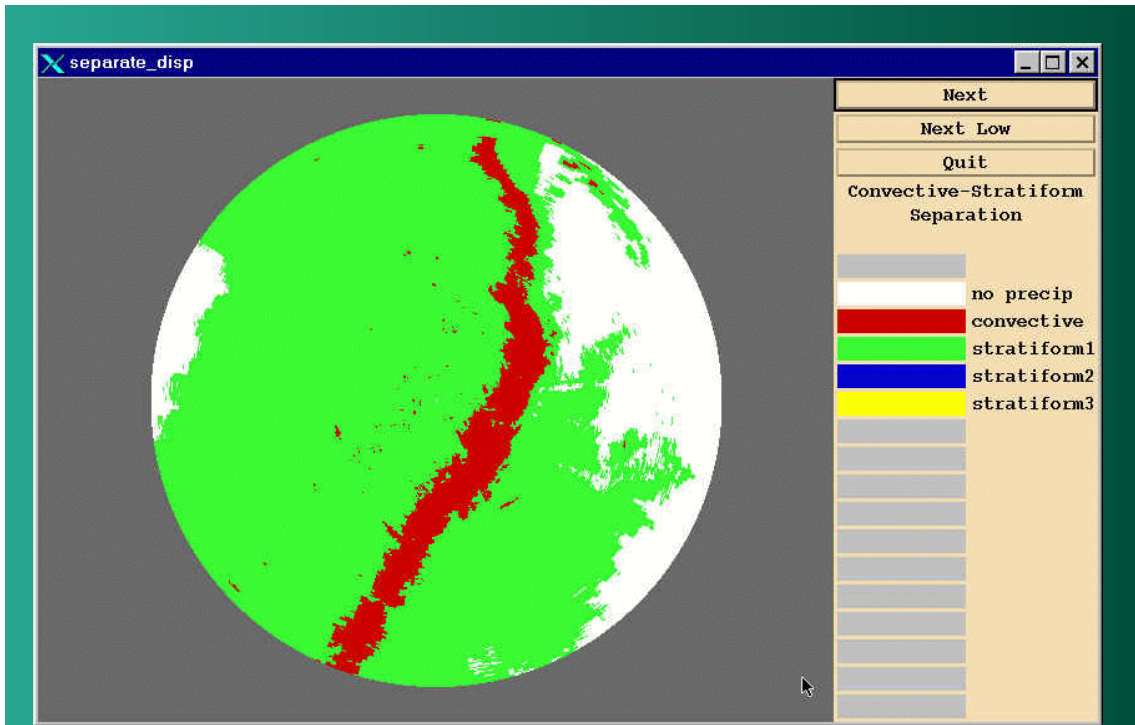


Fig 14 collective separation based on r_x , ρ_{rx} , and ρ_{ht}

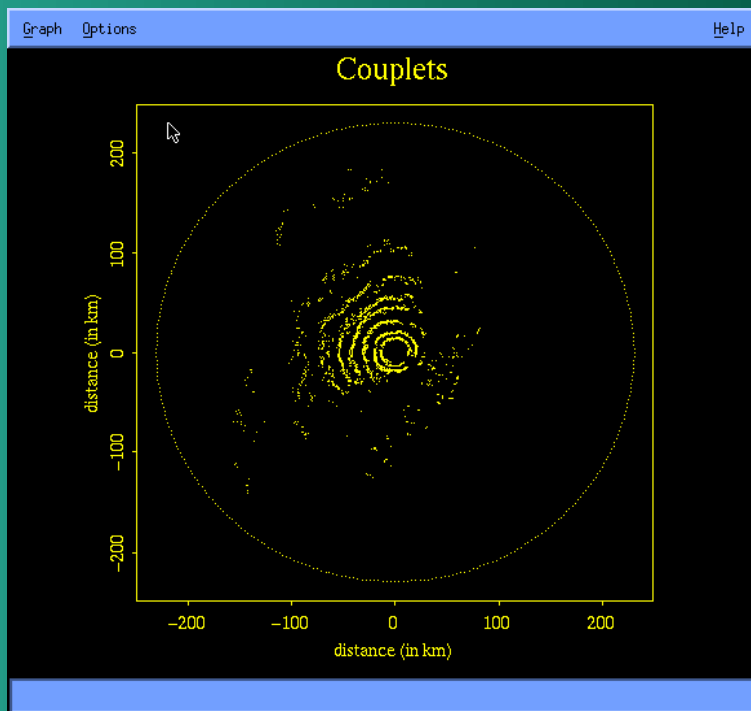


Fig 15 location of couplets

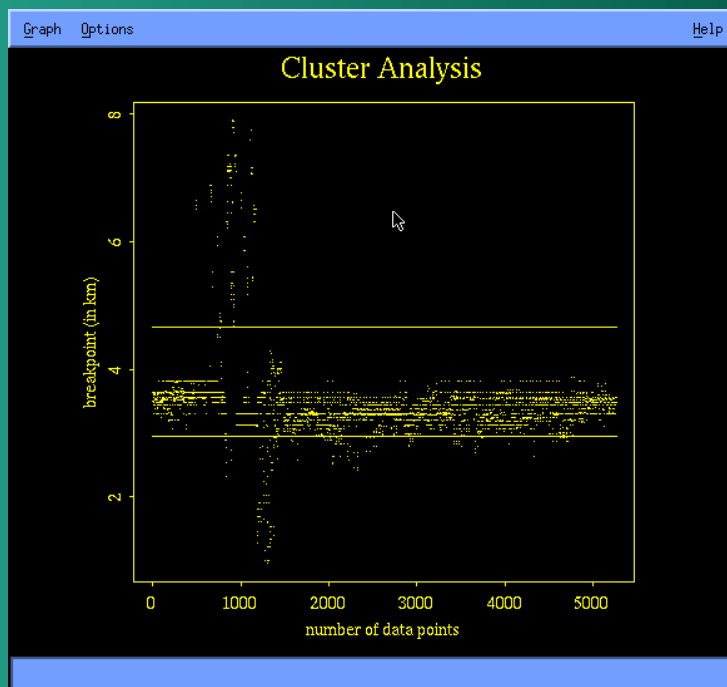


Fig 16 distribution of the height of the couplets and division into clusters

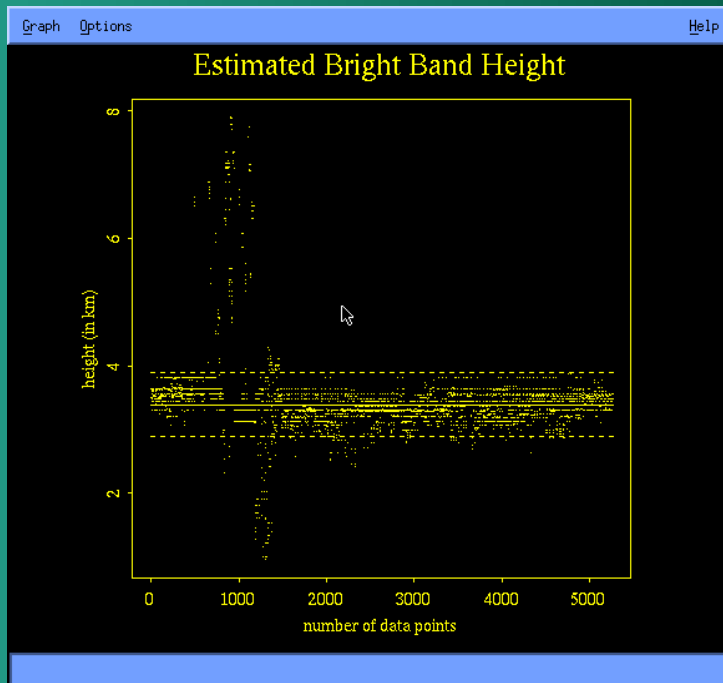


Fig 17 estimated height of the bright band and uncertainty bound

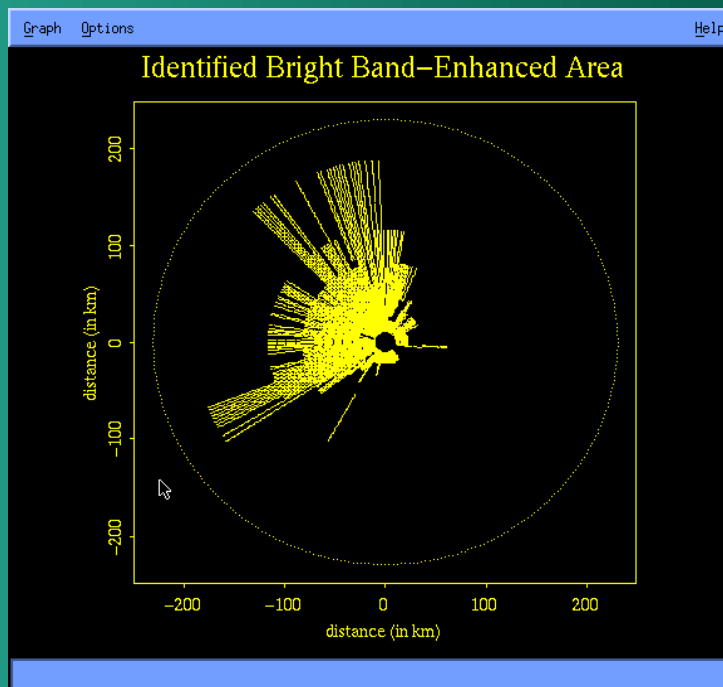


Fig 18 estimated area of bright band enhancement

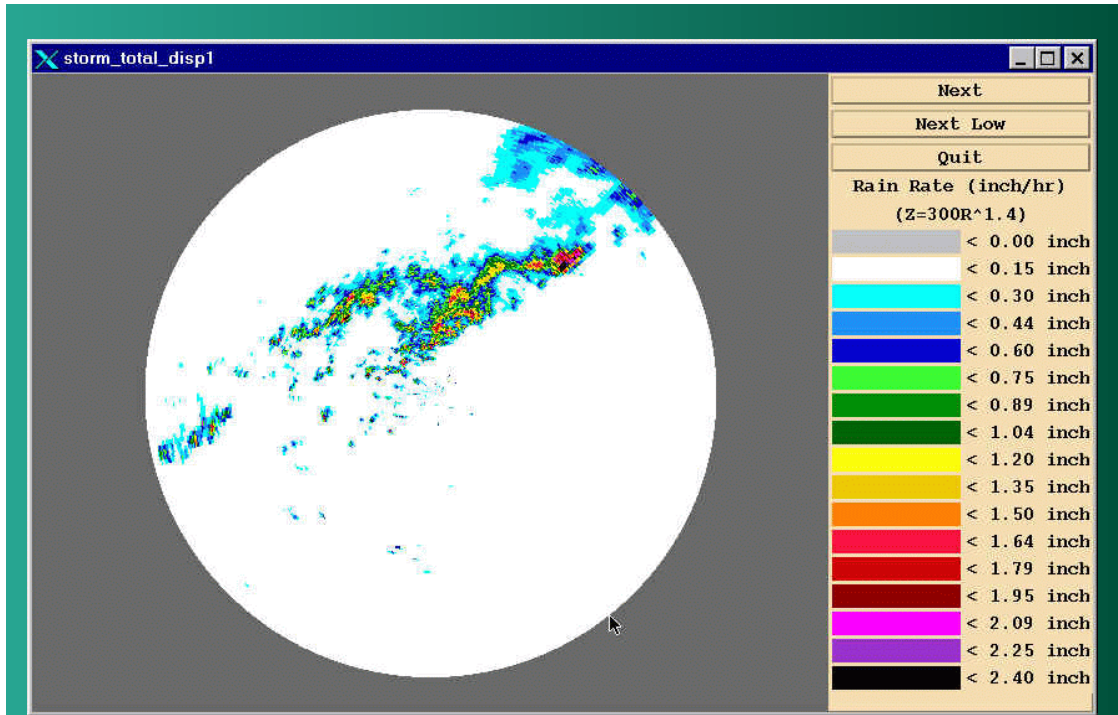


Fig 19 maximum apparent rain rate in the vertical, r_x

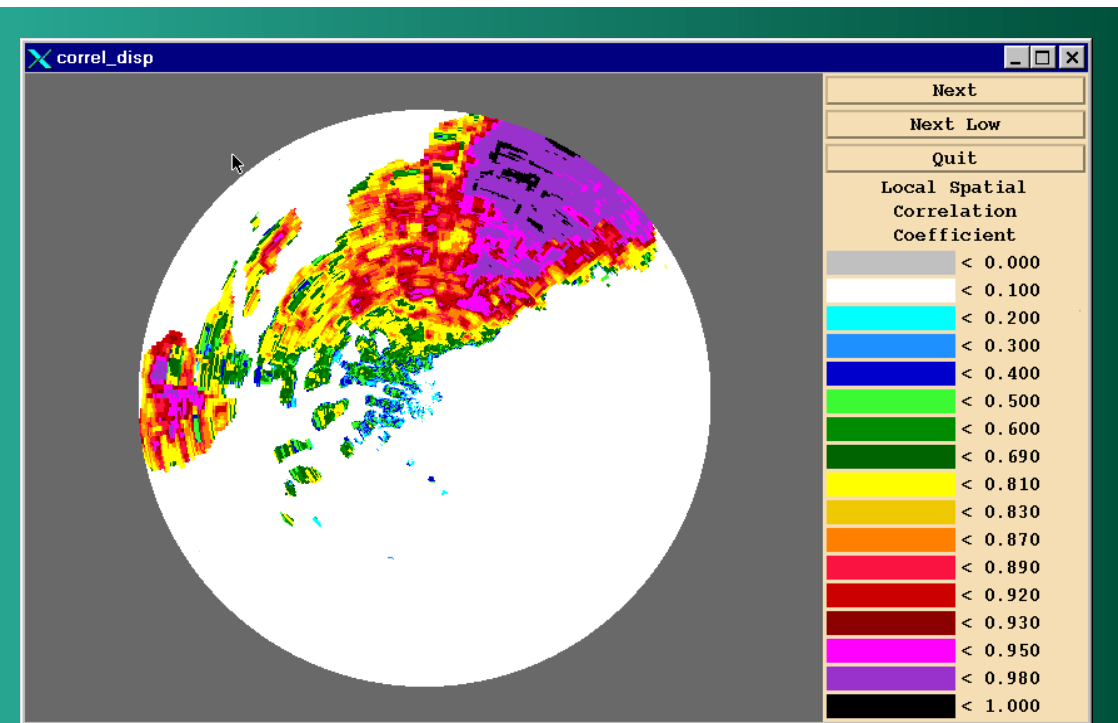


Fig 20 local spatial correlation of r_x , ρ_{rx}

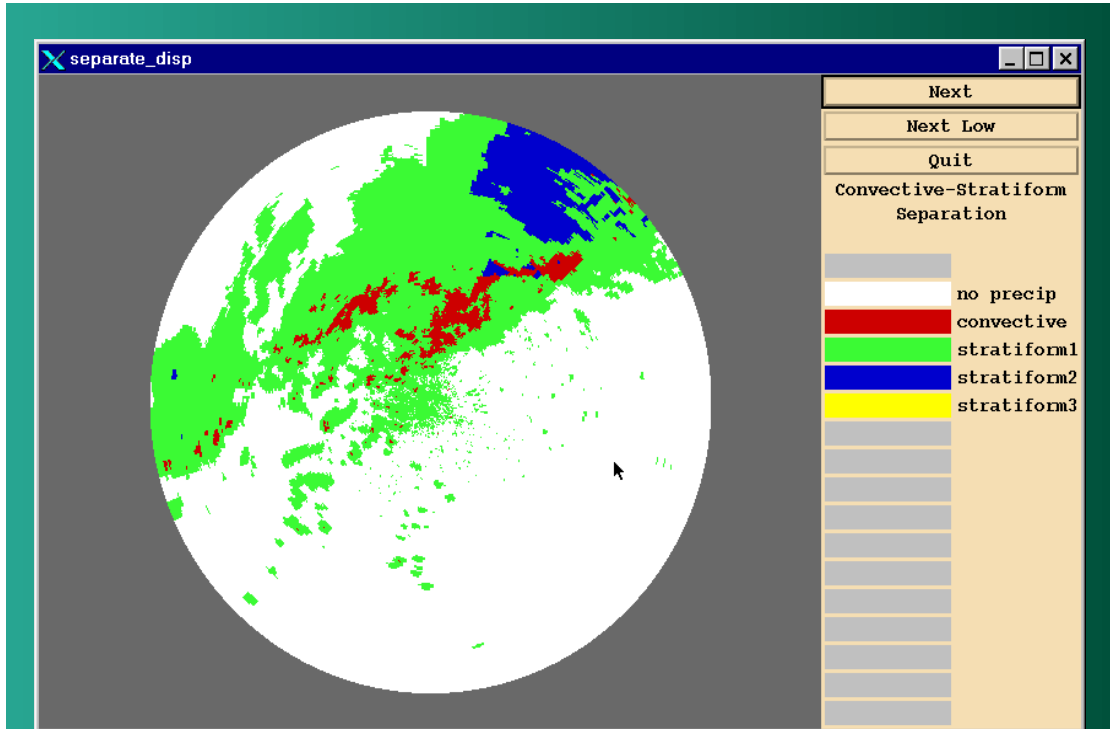


Fig 23 additional separation based on ρ_{rx}

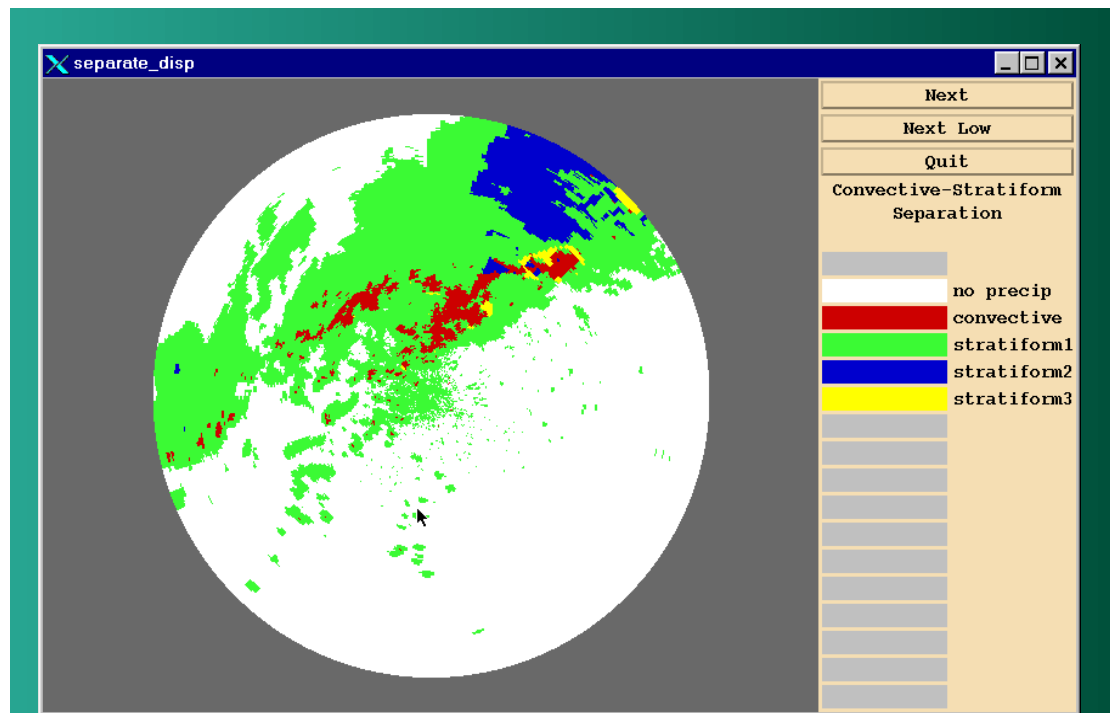


Fig 24 additional separation based on ρ_{ht}

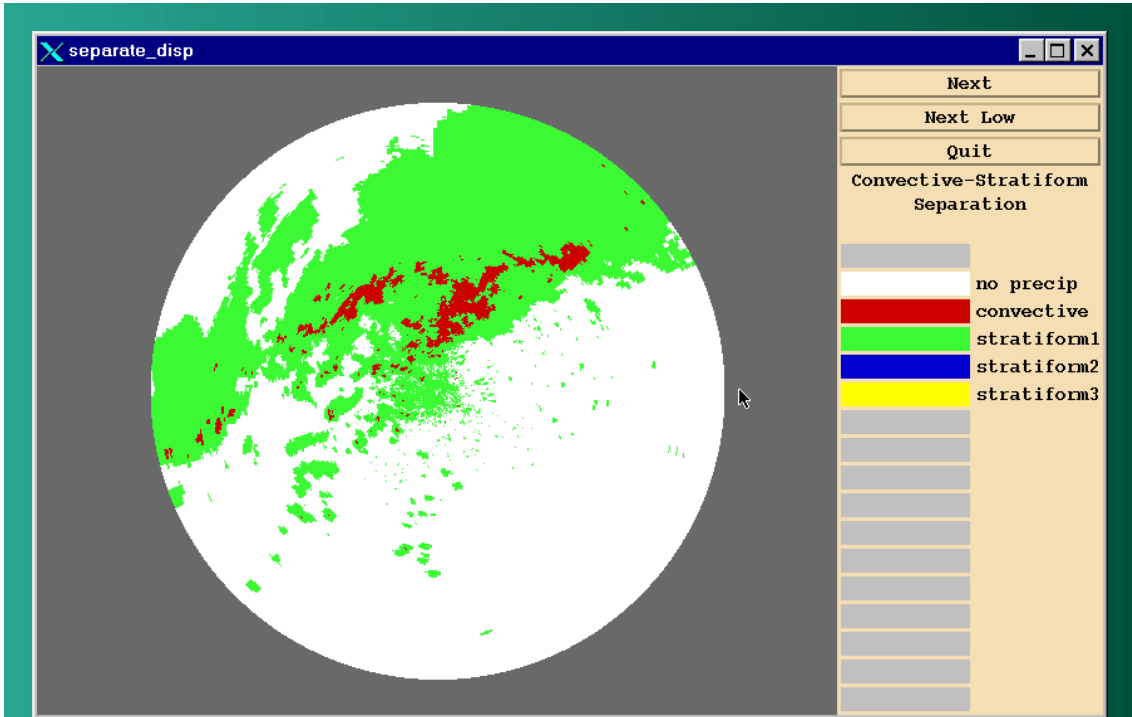


Fig 25 collective separation based on r_x , ρ_{rx} , and ρ_{ht}